JACS
JOURNAL OF THE AMERICAN CHEMICAL SOCIETY

ARTICLE

pubs.acs.org/JACS

High-Performance Hydrogen Production and Oxidation Electrodes with Hydrogenase Supported on Metallic Single-Wall Carbon Nanotube Networks

Draženka Svedružić,[†] Jeffrey L. Blackburn,[‡] Robert C. Tenent,[‡] John-David R. Rocha,[‡] Todd B. Vinzant,[†] Michael J. Heben,[§] and Paul W. King*[,†]

[†]Biosciences Center, and [‡]Chemical and Materials Science Center, National Renewable Energy Laboratory, 1617 Cole Boulevard, Golden, Colorado 80401, United States

[§]Department of Physics and Astronomy, University of Toledo, 2600 Dorr Sreet, Toledo, Ohio 43607, United States

Supporting Information

ABSTRACT: We studied the electrocatalytic activity of an [FeFe]-hydrogenase from *Clostridium acetobutylicum* (CaH2ase) immobilized on single-wall carbon nanotube (SWNT) networks. SWNT networks were prepared on carbon cloth by ultrasonic spraying of suspensions with predetermined ratios of metallic and semiconducting nanotubes. Current densities for both proton reduction and hydrogen oxidation electrocatalytic activities were at least 1 order of magnitude higher when hydrogenase was immobilized onto SWNT networks with high metallic tube (m-SWNT) content in comparison to hydrogenase supported on networks with low metallic tube content or when SWNTs were absent. We conclude that the increase in electrocatalytic activities in the presence of SWNTs was mainly due to the m-SWNT fraction and can be attributed to (i) substantial increases in the active electrode surface area, and (ii) improved electronic coupling between CaH2ase redox-active sites and the electrode surface.

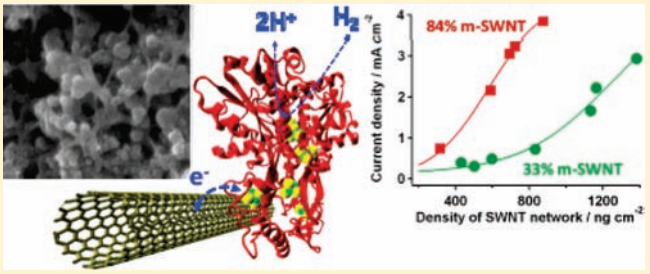

1. INTRODUCTION

Due to the intermittent nature of energy production from sun or wind, energy storage technologies are needed to match energy production and demand cycles. By splitting water into molecular hydrogen (H_2) and oxygen (O_2), the energy harvested by solar-photovoltaic, solar-thermal, or wind technologies can be stored in the form of H_2 as a fuel and used later, on demand, through the electrochemical recombination of H_2 and O_2 in a fuel cell.[1,2] Both processes—water electrolysis and H_2/O_2 utilization—require catalysts to reduce the overpotentials associated with the related electrochemical reactions. To achieve the required current densities, current photoelectrochemical and fuel cell technologies often utilize catalysts composed of platinum-group metals. This dependence on Pt-group catalysts makes scale-up inherently expensive, and the limited supply of metal stocks reduces the potential for wide-scale deployment.[3,4] Synthesis of an efficient H_2 activation catalyst from cheaper, earth abundant elements has been an active field of basic and applied research for decades.[5−7]

Natural evolution has endowed a variety of microbes with the capacity to produce H_2.[8] Hydrogenases (H2ases), the metalloenzymes utilized by these microbes, catalyze the interconversion of molecular hydrogen and protons. The most abundant and best studied examples are the [FeFe] and [NiFe]-H2ases, which are iron−sulfur proteins with bimetallic catalytic clusters containing either two iron atoms or one iron and one nickel atom, respectively.[9] Being comprised of a polypeptide chain and abundant first-row transition metals, H2ases are models for developing cost-effective alternatives to noble metal catalysts for solar-driven H_2 production or fuel cell devices.[10−12] H2ases operate with high turnover numbers at close to zero overpotential and can be reasonably stable,[12,13] as required for practical solar hydrogen conversion or fuel cell applications.

The major challenge for incorporation of H2ases, or any other redox-active enzyme, into a bioelectrical device is the requirement that a robust interaction be established with a conductive support in a manner that allows for efficient electronic interaction but does not compromise catalytic activity.[14−16] Several carbon nanotube (CNT) architectures have been studied as interfaces between H2ases and electrodes, resulting in elevated electrocatalytic activities[13,17−20] and improved stabilities[13] over bulk carbon supports. Nanostructured electrode surfaces have been constructed from either multiwalled[13,20] or single-walled carbon nanotubes,[17,19] and the nanotubes have been aligned as vertical arrays[13] or randomly oriented within films.[17,18] In some cases, H2ase molecules have been immobilized onto surfaces of SWNT

Received: June 10, 2010
Published: March 08, 2011

networks by adsorption,[17,18] whereas other studies used covalent linkages[13,18] or polymer encapsulation[19] to improve electrode performance and stability. Multiwalled CNT scaffolds have also been utilized to construct highly electroactive H_2 electrodes containing a Ni-phosphine synthetic catalyst.[21] According to conventional thinking, unmodified van der Waals surfaces of CNTs (i.e., the walls), like the basal plane of graphite, do not provide functional groups required for enzyme binding and/or enzyme stability.[22,23] Consequently, investigations of CNT-hydrogenase-based electrodes to date have employed tubes that were strongly oxidized, cut, and/or treated with polymers to achieve substantial electrocatalytic activities in the absence of solution-phase redox mediators.[13,17,19,20]

Recently, we showed that [FeFe]-hydrogenase from *Clostridium acetobutylicum* (CaH2ase) has a high affinity for low defect density, unoxidized SWNTs in surfactant stabilized aqueous solutions. The enzyme displaces surfactant and forms an electrically active SWNT/CaH2ase conjugate without introducing functional groups on either SWNT or CaH2ase surface to promote binding. Formation of the SWNT/CaH2ase charge-transfer complex was demonstrated for both the semiconducting (s-SWNT) and metallic (m-SWNT) populations by photoluminescence[24] and Raman spectroscopies,[25] respectively. Though the configuration of the bound enzyme on the nanotube is not currently known, detection of SWNT/CaH2ase charge transfer indicates that at least one of the FeS electron relay clusters is placed in the proximity of the SWNT side wall.

In this contribution we prepared and investigated the electrocatalytic properties of highly active SWNT/CaH2ase-based electrodes. The m- and s-SWNT fractions were separated from as-produced mixtures following the work of Arnold et al.[26] and then used to form electrodes with specific m- and s-SWNT fractions by ultrasonic spraying. In addition to yielding unfunctionalized SWNTs, the separation process rigorously removes amorphous carbon and metal catalyst particles (e.g., Ni, Co) employed in the SWNT synthesis. Throughout the literature, where only partially purified CNT preparations are utilized, potential effects of such impurities on the catalytic properties of a CNT/enzyme-based electrode is often overlooked. In this work, neither the SWNT nor the CaH2ase surface was specially functionalized to facilitate efficient electronic coupling and achieve high electrocatalytic activities. The measured electrocatalytic activities with electrodes with high m-SWNT content matched those of Pt-group metals and other non-noble metal catalysts at neutral pH[27] and exceeded the activities measured for other H2ase-based electrodes in both proton reduction and H_2 oxidation. To our knowledge, this is the first study to explore the role of SWNT conductivity type in electrocatalysis, and the first to consider the impact of m-SWNT content in the design of highly electroactive enzyme-based electrodes with potential for application in a variety of technologies.[28]

2. EXPERIMENTAL SECTION

Preparation and Formation of SWNT Networks. Single-walled carbon nanotubes (SWNT) with average diameters of ~1.3 nm were prepared by laser vaporization, and s- and m-SWNT enriched dispersions were prepared by density gradient ultracentrifugation (DGU), as described previously.[26,29] Briefly, raw laser vaporized (LV) SWNTs were dispersed in the appropriate cosurfactant mixture and injected near their isopycnic point in a density gradient formed with an iodixanol/water mixture. The cosurfactant mixture for m-SWNT enrichment was 3:2 sodium dodecyl sulfate and sodium cholate (SDS/SC) and for s-SWNT enrichment was 4:1 SC/SDS (both 2% total surfactant concentration). DGU separation was performed in an SW-41 rotor (LX-100P Beckman centrifuge) at a speed of 41×10^3 rpm for 12−16 h.

Following DGU separation, the ratio of m-SWNTs to s-SWNTs was determined for fractional aliquots by absorbance spectroscopy (see Supporting Information, Figure S1), using the areas underneath the first metallic (M_{11}) and second semiconducting (S_{22}) peak envelopes, as described previously.[30] A number of fractions were combined to provide volumes (10−30 mL) with selected m-SWNT/s-SWNT ratios. These samples were then dialyzed against an aqueous solution of 3:2 SDS/SC (2% total concentration) to remove iodixanol and to provide a suitable ink for ultrasonic spraying. Following dialysis, the samples were centrifuged at 6000 rpm in a SW-32 rotor for 1 h to remove poorly suspended SWNTs and precipitated iodixanol and surfactant. Electrodes were prepared by spraying the dialyzed SWNT inks with predetermined s-/m-SWNT ratios onto carbon cloth (C-cloth) (A1NC ECC, BASF Fuel Cell, Inc.). Spraying was done with a custom-built spraying system which employs a Sono-Tek ultrasonic spray head, as described previously.[31] After spraying, the electrodes were soaked overnight in 4 M nitric acid to remove surfactants. The number of spray passes and the SWNT concentration in solution provided precise control over the SWNT coverage ($\mu g\ cm^{-2}$) on the C-cloth. To verify SWNT coverage, a glass witness slide was sprayed simultaneously and measured by absorbance spectroscopy following surfactant removal by nitric acid.[30,31] A series of electrodes were prepared for each m-/s-SWNT ratio with a maximum SWNT coverage of ~2 $\mu g\ cm^{-2}$. Scanning electron microscopy (SEM) images were obtained as previously described.[32]

Preparation and Characterization of Hydrogenase and Electrochemical Methods. Recombinant [FeFe]-hydrogenase from *C. acetobutylicum* (CaH2ase) was expressed in *Escherichia coli* and purified according to previously reported procedures.[33] The CaH2ase activity for H_2 evolution was measured by titration with 25 mM reduced methyl viologen (MV) as an electron donor, according to an enzyme activity assay previously described in the literature.[11] Protein concentrations were determined using a Qubit fluorometer and Quant-iTTM protein assay kit (Molecular ProbesTM, Invitrogen). The specific activities of the two CaH2ase preparations used here were 90 ± 10 and 140 ± 9 U mg^{-1} (1 U of activity is defined as 1 μmol of H_2 per minute).

Cyclic voltammetry was performed with a CH Instruments 600C electrochemical analyzer/workstation using a platinum wire (Alfa Aesar) counter electrode and silver−silver chloride reference electrode (Bioanalytical Systems, Inc.). All potentials were referenced against the Ag/AgCl (3 M NaCl) reference electrode, which has a potential of −0.209 V vs the Standard Hydrogen Electrode (SHE). All electrochemical experiments were performed in a 100 mM *N*-tris(hydroxymethyl)methyl-2-aminoethanesulfonic acid (TES) buffer at pH 7. TES was obtained from Sigma-Aldrich and used as received. Pyrolytic graphite (PG) and glassy carbon (GC) electrodes (ALS Co., Ltd.) were polished with emery paper and briefly sonicated in doubly distilled water prior to use. C-cloth electrodes either bare or with SWNT networks were cut into pieces with a geometrical surface area of 0.09 cm^2 and glued to the surface of polished vitreous carbon electrodes with conductive carbon paint (SPI, West Chester, PA).[34] CaH2ase was handled and all electrochemistry experiments were performed under strictly anaerobic conditions under either a 3−4% H_2 (balance nitrogen) or a 100% H_2 atmosphere to avoid irreversible inactivation by molecular oxygen.[25] The enzyme was immobilized on the electrode surface by soaking the electrode in 50 μL of enzyme solution with total protein content ~0.3 mg mL^{-1} for 2 h. The electrode was removed from solution, rinsed well with deionized water, and transferred to fresh buffer solution for electrochemical characterization. Cyclic voltammograms (CVs) were obtained at 23 °C with both stationary and rotating electrodes, and potential

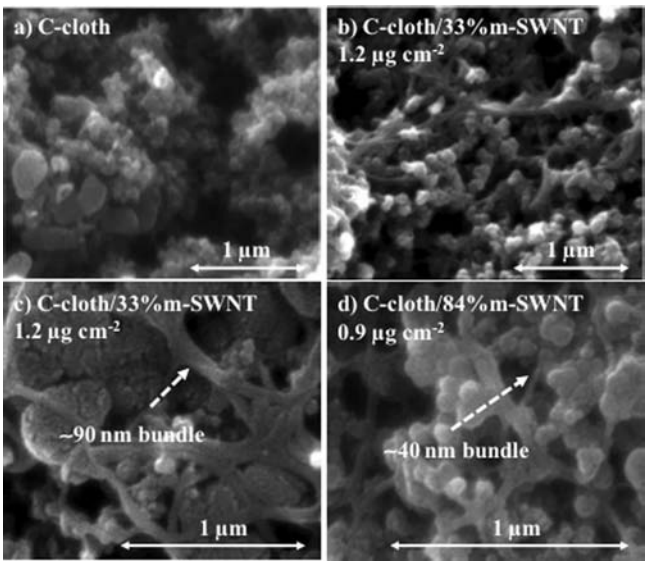

Figure 1. SEM images of the electrodes surfaces: (a) C-cloth, (b) and (c) C-cloth/SWNT with 33% m-SWNT content and an areal density SWNT network of 1.2 μg cm^{-2}, and (d) C-cloth/SWNT with 84% m-SWNT content, 0.9 μg cm^{-2}. Images recorded with magnification of 100,000.

scans were initiated at the most positive potential. Current densities for all electrodes used in this work are reported by dividing the measured current by the geometric surface area of the electrode. For the data analysis, catalytic CVs were background corrected by subtracting the CVs measured without adsorbed CaH2ase under the identical conditions.

The electrochemically active surface areas were evaluated by determining the capacitance of the electrodes from CVs measured without adsorbed CaH2ase at varying sweep rates (1−200 mV s^{-1}) in the 100 mM TES buffer within a potential range in which there was no significant Faradaic current, typically between −1 and −0.6 V. The measured current was plotted as a function of the sweep rate, and the electrode capacitance was determined from the slope of the curve.[34,35]

3. RESULTS AND DISCUSSION

Electrode Morphology. Scanning electron microscopy (SEM) was used to analyze the surface morphology of bare C-cloth and C-cloth/SWNT electrodes. A few angstroms of iridium were applied by sputtering to eliminate charging effects during imaging. Images of the bare C-cloth showed particles ranging in size from tens to hundreds of nanometers agglomerated into larger features with considerable roughness on the micrometer scale (Figure 1a). Application of small amounts of SWNTs by spraying did not significantly alter the surface morphology. For example, Figure 1b,c shows the surface after application of 1.2 μg cm^{-2} of nanotubes with a 33% m-SWNT content on the C-cloth support. The images of Figure 1a and 1b are qualitatively quite similar except for the presence of a few thin strands of SWNTs in the latter image. Figure 1d shows the morphology for a 0.9 μg cm^{-2} network of 84% m-SWNTs on the C-cloth support. The overall electrode morphology is clearly dominated by the C-cloth, but thin SWNT bundles ranging in size between ~20−110 nm can be seen contacting and bridging between C-cloth particles, suggesting good electrical contact between the two. Additional SEM images are given in the Supporting Information (Figure S2).

Electrochemical Characterization. To understand the catalytic performance of CaH2ase supported on SWNT, we measured CVs for all C-cloth and C-cloth/SWNT electrodes with and without adsorbed CaH2ase. In general, the shape of a catalytic CV measured with adsorbed CaH2ase could be understood as a superposition of capacitive currents, due to the charging of the electrical double layer at the electrode/electrolyte interface, and Faradaic currents due to charge transfer reactions associated with the CaH2ase catalytic activities. Background CVs obtained under identical conditions in the absence of CaH2ase were valuable for assessing the capacitance of the electrode, which in turn provided an estimate of the electrochemically active surface area (vide infra). During the course of this work all catalytic CVs were presented as "background corrected" to make clear the electrode's electrocatalytic activity (an example is given in Figure S3). This approach does not accurately remove all effects of electrode capacitance on catalytic CV since electrode capacitance should also be affected by the presence of the adsorbed protein layer. Nevertheless, background-correction was useful to compensate for the dominant contributions to the capacitive currents for the different types and preparations of electrodes.

Catalytic Activities of C-cloth/SWNT/CaH2ase Electrodes. Native CaH2ase was adsorbed onto bare C-cloth electrode or C-cloth/SWNT electrodes with varying m-SWNT content. Catalytic CVs of CaH2ase adsorbed on electrodes prepared from bulk carbon have been described previously.[11] The point of zero potential equates to the formal potential of H^+/H_2 couple under the applied experimental conditions, which can be calculated using the Nernst equation. The negative (cathodic) current corresponds to proton reduction, while the positive (anodic) current corresponds to H_2 oxidation, both catalyzed by CaH2ase immobilized onto the electrode surface. In order to measure anodic currents, higher concentrations of H_2 are required (typically experiments are performed under 100% H_2) and the working electrode is rotated at high speeds to overcome mass transport limitations. The CVs in Figure 2 show that both the proton reduction and H_2 oxidation currents obtained for a C-cloth/SWNT electrode (84% m-SWNT, areal density ~0.7 μg cm^{-2}) were enhanced by more than 200-fold as compared to a bare C-cloth electrode. Under the applied conditions (pH 7, 100% H_2, 5000 rpm), the point of zero current for C-cloth/CaH2ase and C-cloth/SWNT/CaH2ase electrodes (from Figure 2) were reached at potentials of −0.633 and -0.622 vs Ag/AgCl (3 M NaCl) respectively, values that are close to the calculated Nernstian value of −0.6215 V vs Ag/AgCl (3 M NaCl) for the H^+/H_2 couple. This result shows that the presence of the SWNT network does not significantly alter the CaH2ase operating potential or H^+/H_2 equilibrium on the electrode surface. The small deviations from the calculated value might be due to a small drift in the pH or H_2 partial pressure at the electrode surface or incomplete removal of the capacitative currents. In contrast to the H_2 oxidation activities which were measured under 100% H_2 with a rotating working electrode (Figure 2), the proton reduction activities were similar in value regardless of whether the working electrode was stationary under 3−4% H2 (Figure 2, dashed red line) or rotated under 100% H2 (Figure 2, full red line). Consequently, proton reduction processes could also be straightforwardly studied without electrode rotation.

Figure 3 compares background corrected proton reduction currents for CaH2ase adsorbed on bare C-cloth and C-cloth/SWNT electrodes with varying m-SWNT content. As shown previously in Figure 2, the bare C-cloth electrode treated with CaH2ase shows very little cathodic activity above the capacitive

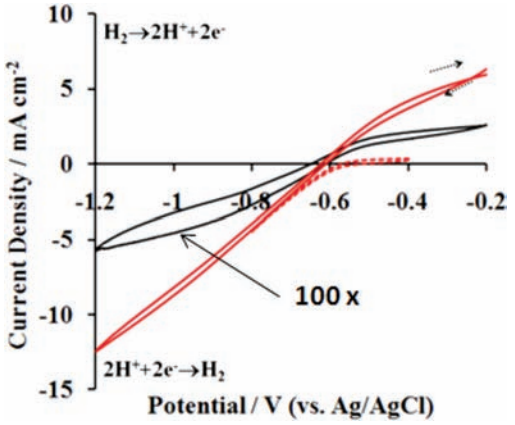

Figure 2. Catalytic CVs for CaH2ase adsorbed on surface of C-cloth (black) or C-cloth/SWNT electrodes (84% m-SWNT, areal density ~0.7 μg cm^{-2} [red]). Currents measured with C-cloth electrode are multiplied by 100 for easier comparison. Working electrode rotated at 5000 rpm, 100% H_2 (full line) or 0 rpm, 3−4% H_2 (dashed line). CaH2ase specific activity, 140 U mg^{-1}. Scan rate, 20 mV s^{-1}. Arrows indicate scan direction. Potential can be converted to SHE scale by adding +0.209 V.

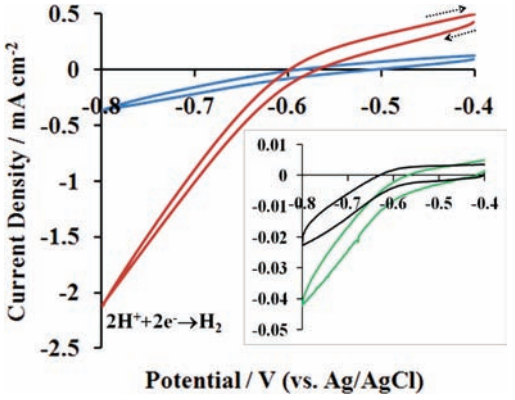

Figure 3. Catalytic CVs for CaH2ase adsorbed on the surface of C-cloth (black) or C-cloth/SWNT electrodes with areal density ~0.5 μg cm^{-2} and m-SWNT content of: 33% (green), 45% (blue) and 84% (red). Working electrode was not rotated, 3−4% H_2 partial pressure. CaH2ase specific activity, 90 U mg^{-1}. Scan rate, 20 mV s^{-1}. Arrows indicate scan direction. Potential can be converted to SHE scale by adding +0.209 V. Inset: zoom on C-cloth and C-cloth/33% m-SWNT.

currents. Evidently, any CaH2ase present on the C-cloth surface does not participate significantly in electrocatalysis. Thus, adsorbed enzyme is not electrically connected to the bulk of the C-cloth electrode and/or improperly aligned for efficient electronic coupling with the electrode surface. The SEM images suggest that many of the carbon particles comprising the C-cloth may not be in good electrical communication with the overall electrode. However, as shown in Figures 2 and 3, modification of C-cloth electrodes with SWNTs produces dramatic increases in the catalytic currents with adsorbed CaH2ase. Moreover, for electrodes with similar SWNT areal densities (~0.5 μg cm^{-2}) the magnitude of the increase clearly correlates with the m-SWNT content.

Figure 4 shows how the performance of CaH2ase-based electrodes depends on the amount of sprayed SWNTs. Here, the background corrected cathodic current density at −0.8 V was plotted

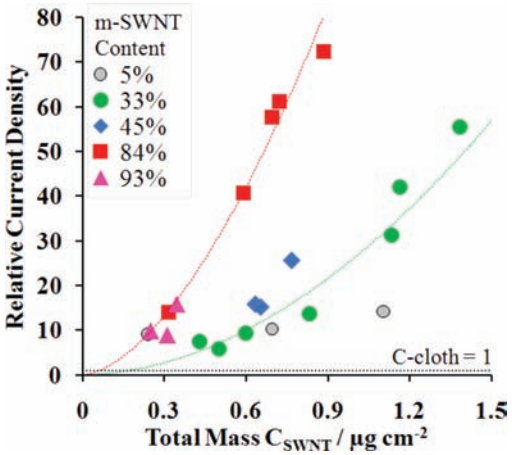

Figure 4. Proton reduction current densities measured at −0.8 V (vs. Ag/AgCl) for C-cloth/SWNT/CaH2ase relative to the proton reduction current density measured for C-cloth/CaH2ase electrode under the same conditions (RPRC). Plot shows the increase in RPRC as a function of SWNT coverage for networks with different m-SWNT content (color-coded). Experimental conditions are the same as described for the Figure 3. Lines have been added to guide the eye. Measurements were done in duplicate or triplicate with an average standard error of ±0.16 mA cm^{-2}. The CaH2ase specific activity was 90 U mg^{-1}.

as function of SWNT coverage for networks having different m-SWNT contents. Once again, it is clear that the films with higher m-SWNT contents support larger catalytic currents at a fixed SWNT coverage. Additionally, the current density is observed to increase with the amount of sprayed SWNTs for all m-SWNT contents. The change in current density with coverage is the greatest for the highest m-SWNT content networks. In contrast, the current is only modestly improved with increasing coverage for 5% m-SWNT networks. Previously, our Raman spectroscopy study showed that CaH2ase displaces surfactant, spontaneously binds to and forms charge transfer complexes with both m- and s-SWNTs in solution.[24,25] The results presented here can be explained by considering that CaH2ase on s-SWNTs do not contribute to externally measured catalytic currents to the same extent as CaH2ase on m-SWNTs, possibly because s-SWNTs do not make a good electrical contact to the underlying C-cloth support due to their inherent semiconducting structure. In contrast, m-SWNTs are able to make a good electrical contact with the C-cloth due to the relatively high concentration of free carriers near the Fermi energy.

Effects of SWNT Networks on Electrode Surface Area. To develop a simple assessment of how SWNT networks increase the surface area of electrodes we consider the networks to consist of representative (10,10) SWNTs with diameters of 1.36 nm.[36] The SWNTs in the bundles observed in the SEM images (Figure 1) appear to be close-packed, so the lattice parameter of the original lattice can be taken as 1.68 nm and, thus, the carbon density in the bundles is 1.33 g cm^{-2}.[36] Considering 500-tube and 2600-tube circular bundles having diameters corresponding to those typically observed by SEM (~40 and ~90 nm, respectively − Figure 1), we calculate that ~0.76 cm^2 and ~0.34 cm^2 of new SWNT surface area, respectively, is added for each 1 μg of sprayed SWNTs. Note that this analysis is consistent with that of Peigney et al.[37] and underpins a "rule of thumb" that will be useful here; ~1 cm^2 of new surface area is produced when 1 μg of SWNTs is sprayed-deposited. For completeness, we note that the external surface

dx.doi.org/10.1021/ja104785e |J. Am. Chem. Soc. 2011, 133, 4299–4306

area of 1 μg of individual, unbundled (10,10) tubes would not be tremendously larger ($\sim$17 cm^2).

To determine the electroactive surface area of the C-cloth electrode we analyzed the background CVs taken with bare C-cloth at several scan rates according to $i_c = C\,dV/dt$ where i_c is the capacitive charging current, dV/dt is the scan rate, and C is the double layer capacitance (for specific examples see Supporting Information Figure S4a,b). Carbon cloth is reported to have a specific capacitance of $\sim$2 μF cm^{-2} in a variety of different electrolytes.[38] Using this value and the value for C determined from a linear fit to a plot of i_c vs dV/dt for eight different scan rates between 2 and 200 mV/s, the ratio of electroactive to geometric surface area for our bare C-cloth electrodes can be estimated to be $\sim$43.

Returning to Figures 2−4, we can now conclude that dramatic enhancements in catalytic currents occur with very little addition of new surface area. For example, at a sprayed SWNT coverage of 2 μg cm^{-2}, only $\sim$2 cm^2 of SWNT surface sits on top of $\sim$43 cm^2 of electrochemically active C-cloth (within a 1 cm^2 geometric projection). Evidently, the small amount of SWNT surface is very effective at interfacing CaH2ase to the underlying C-Cloth. To test the veracity of our analysis we considered whether sufficient SWNT surface area was present to bind enough enzymes to support the observed catalytic currents. Considering the CaH2ase turnover number to be 20,000 per second[39] and the projected surface area of a single CaH2ase molecule to be 60 nm^2 (based on the crystal structure[40]), we can calculate that $\sim$0.6 cm^2 of the electrode surface would need to be covered with catalytically active CaH2ase molecules to support the observed proton reduction activities (i.e., $\sim$10 mA cm^{-2}). Thus, there appears to be more than enough space on the SWNT to bind the needed CaH2ase operating at high turnover numbers. The analysis also reinforces the idea that defect-free SWNTs can bind and make electrical contact to CaH2ase through strict physisorption interactions. If this was not the case, and oxygenated SWNT carbon species were required to bind sufficient enzyme to support the observed currents, the surface concentration of defects would be so high that the characteristic electronic and morphological structure of SWNTs would likely be disrupted, which is not observed. In summary, even though SWNT networks have only minor contribution to the overall electrode surface area, the nanotube presence dramatically increases the electrocatalytic performance of the CaH2ase-electrode.

Relationship Between Electroactive Surface Area and Proton Reduction Activity. In general, increases in electrocatalytic activity of an enzyme-based electrode depend on increases in enzyme electroactive coverage.[39,41] In the absence of redox mediators, only the CaH2ase molecules that are adsorbed on a conductive portion of the electrode surface in orientations that place the redox centers within an electron tunneling distance to/from the electrode can undergo direct electron transfer and therefore contribute to observed catalytic currents. In this section we will discuss further possible effects of SWNT networks on the observed catalytic currents and CaH2ase electroactive coverages.

Combining the simple geometric analysis of the SWNT surface area with a determination of the electroactive surface area of the C-cloth offers some understanding of the factors affecting the enzyme catalyzed proton reduction. However, a more complicated picture emerges if the electroactive surface area for each C-cloth/SWNT electrode is considered. This more detailed analysis was motivated by the observation that CVs of C-cloth/SWNT electrodes in the absence of CaH2ase showed large capacitive charging currents at the higher SWNT coverages. Because the specific capacitances of the different m- and s-SWNT species and the equivalent circuit describing how the SWNTs are connected with the C-cloth substrate are not known at this time, we are limited to performing a relative analysis which implicitly assumes that each electrode has a single surface in contact with the electrolyte and a single value for the specific capacitance associated with all portions of that surface. Figure 5 shows the relative electroactive surface area (RESA) for C-cloth/84% m-SWNT electrode as a function of SWNT coverage. Data points were determined by dividing the capacitance measured for each electrode by the capacitance of the bare C-cloth electrode. The capacitance measurements for the C-cloth/SWNT electrodes were performed as previously described with at least four scan rates. In general, scan rates slower than 100 mV s^{-1} were required to obtain a linear fit to the i_c vs dV/dt data (Figure S4). Also plotted in Figure 5 for comparison are the relative proton reduction currents (RPRCs) at −0.8 V, which are the measured proton reduction currents with adsorbed CaH2ase for each electrode divided by the proton reduction current measured for the C-cloth/CaH2ase electrode. Figure 5 shows that at low SWNT coverages (<1 μg cm^{-2}, $\sim$50 spray cycles) the RPRC value increases much more quickly with coverage than does the RESA. This result is consistent with the simple model presented earlier which views the added SWNT area to be relatively small and considers that only m-SWNT surfaces can efficiently bind and electrically connect catalytically active CaH2ase. At higher coverages (> 50 spray cycles), the RPRCs and RESAs increase in parallel. The delayed onset for the increase in the RESA can be explained if one considers that many of the carbon particles observed by SEM on the C-cloth electrode are electrically disconnected. Initially, only a fraction of the small amounts of added nanotubes become electrically active when they land and contact carbon particles that happen to already be connected. We estimate the length of the individual nanotubes in the ink to be $\sim$800 nm,[31] so nearby particles may be out of reach from one another until a network

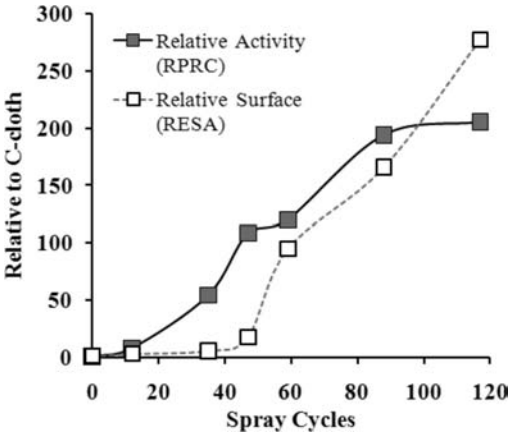

Figure 5. Changes in the relative electroactive surface area (RESA) and relative proton reduction current (RPRC) with adsorbed CaH2ase, measured at −0.8 V) of a C-cloth/SWNT (84% m-SWNT) electrode are plotted against increased SWNT coverage. Electrodes with increased areal density of SWNT networks were achieved by multiple spraying of SWNT suspension. 100 spray cycles corresponds roughly to 2 μg cm^{-2}. Experimental conditions are the same as described for the Figure 3. Lines have been added to guide the eye.

dx.doi.org/10.1021/ja104785e |J. Am. Chem. Soc. 2011, 133, 4299–4306

of nanotube bridges can be developed. As more nanotubes are deposited, electrically isolated particles may be connected to other well-connected particles by the nanotubes, giving rise to increased electroactive surface area. The percolation threshold for electrical conduction in relatively flat films comprised of nanotubes like those used here is ~0.011 μg cm^{-2}.[31] It makes sense that a substantially larger surface concentration (1 μg cm^{-2}) may be required to develop percolation over significantly rougher terrain.

In contrast to the delayed onset observed for the RESA, the RPRC for the C-cloth/84% m-SWNT electrodes start and continue to increase in a nearly linear fashion with increasing SWNT coverage with the values higher than the RESA values (Figure 5). Therefore it can be concluded that the effects of SWNT on the RESA is not the only contributing factor to the increase in RPRC. As noted earlier, at low coverages, poorly integrated SWNT networks do not contribute significantly to the overall electrode electroactive surface and therefore to the electroactive surface available for CaH2ase binding. Alternatively, individual SWNTs might promote orientation of CaH2ase molecules adsorbed on the electrically active carbon particles in a way that allows efficient electronic coupling between the CaH2ase redox clusters and the electrode surface. As SWNT coverage and the overall electroactive surface area increases it is likely that this *orientation* effect will be less significant and increase in RPRC will reflect more closely increase in RESA. The roll-off in RPRC above >80 spray cycles (Figure 5) is difficult to explain when one considers that the RESA is still increasing. Possibly, all of the current is being routed through just a relatively small number of carbon particles comprising the C-cloth and, with current densities being quite high, electrical resistance limitations may be manifested. A proposed model for the interaction between C-cloth, SWNTs and CaH2ase molecules is illustrated in Figure S5. It is also important to note that some SWNTs can reside in crevices too small in dimension for the CaH2ase molecule to adsorb. These tubes will have an impact on the overall RESA value but not on the CaH2ase interaction with the electrode surface and the RPRC value.

Comparison of C-cloth/SWNT Electrodes with Other Commonly Used Carbon Electrodes. As we have shown previously, through the addition of the SWNT networks, even poor electrode materials for CaH2ase immobilization, such as C-cloth, can be readily transformed into a highly electroactive surface. This is an important observation as one might envision a device for direct conversion of sunlight to H_2 where an H2ase, or another molecular catalyst, is interfaced through a SWNT network to a bulk material otherwise unsuitable for catalyst immobilization and charge transfer. Nevertheless, the bare C-cloth might not adequately reflect other carbon materials commonly utilized for the design of H2ase-based electrodes. To benchmark the electrocatalytic performance of our best C-cloth/SWNT electrode with adsorbed CaH2ase against the performances of other carbon materials we measured the proton reduction electrocatalytic activities of basal plane, edge plane pyrolytic graphite (BPG and EPG respectively) and glassy carbon (GC) electrodes at −1.2 V (vs Ag/AgCl) (Figure 6). All the experiments were performed with the same CaH2ase preparation and under the identical experimental conditions to achieve the most meaningful comparison. In this set of experiments, the 84% m-SWNT electrode (~2 μg cm^{-2}) showed a proton reduction current of 12 mA cm^{-2}, more than 200-fold above that of the bare C-cloth electrode, and 6 to

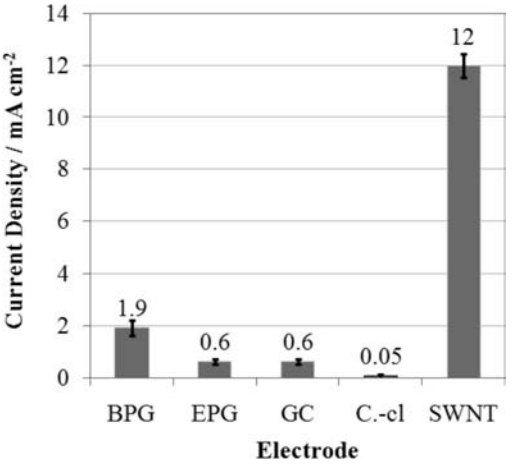

Figure 6. Comparison of proton reduction current densities at −1.2 V vs Ag/AgCl for CaH2ase immobilized on different carbon electrodes: pyrolytic graphite basal (BPG) and edge (EPG) plane, glassy carbon (GC), C-cloth (C-cl.) and C-cloth/SWNT (84% m-SWNT, ~2 μg cm^{-2}) (SWNT). CaH2ase specific activity was 140 U mg^{-1}.

20-fold above the performance of the BPG, EPG, and GC electrodes. To better correlate electrode material to capacitance and electrocatalytic activities measurements, RESAs for other carbon electrode materials were also determined. The results summarized in Table S1 suggest that differences in the electrocatalytic activities for different carbon electrodes (Figure 6) are at least partially due to the differences in electroactive surfaces. In the case of the BPG electrode, the increase in electrocatalytic activity is greater than the increase in the electroactive surface, which suggests that the chemical nature of the BPG electrode might be more favorable to CaH2ase binding. The GC electrode was found to have similar electrocatalytic activity as EPG, but higher RESA, suggesting it has the least CaH2ase accessible surface morphology.

Comparison of C-cloth/SWNT/CaH2ase Electrocatalytic Activities with Literature. It is important to note that most literature reports of H2ases immobilized on different CNT frameworks have primarily shown enhanced H_2 *oxidation* catalysis.[13,17,18] With the C-cloth/SWNT/CaH2ase (84% m-SWNT, ~0.7 μg cm^{-2}) electrode we demonstrate ~3-fold increase in the estimated H_2 oxidation currents above the highest reported H_2 oxidation current density, which was measured for a [NiFe]-H2ase immobilized on multiwalled CNT forests grown on a gold surface.[13] This comparison is based on the H_2 oxidation limiting currents estimated under absence of mass transfer limitations determined in this work (Figure S6) and the value reported by Alonso-Lomillo and co-workers.[13] Additionally, our electrodes show the highest reported H_2 *production* activities for any H2ase-based electrode reported so far. LeGoff and co-workers[21] have shown that high current densities can also be achieved for both proton reduction and H_2 oxidation with a synthetic nickel bisdiphosphine catalyst under strictly acidic conditions. The values of 2 mA cm^{-2} at −0.7 and +0.2 V (vs Ag/AgCl) reported by LeGoff et al. are lower than the values of 3 and 6 mA cm^{-2}, respectively, achieved here at the same potentials. Moreover, it is important to note that our C-cloth/SWNT electrodes were not fully optimized. Higher current densities might be achieved through several routes including, for example, utilization of SWNT networks with even higher areal density and m-SWNT content,

optimization of the conductive support used for the SWNT immobilization, and utilization of H2ase preparations with higher specific activities.[42]

Stability of C-cloth/SWNT/CaH2ase Electrodes. We have observed that the stability of the immobilized SWNT networks depends on the support material and the network preparation procedure. For example, SWNT networks may be prepared by simply applying a drop of a SWNT suspension to the surface of PG or GC electrodes and leaving it to dry, as previously reported in the literature.[17] With this approach we achieved high current densities (higher than the values reported in this paper) but results were irreproducible (data not shown). In contrast, the SWNT networks prepared by ultrasonic spraying on C-cloth surface gave reproducible results and electrodes with high stability.

The catalytic performance of adsorbed CaH2ase films on C-cloth/SWNT electrodes was stable when kept in the buffer (100 mM TES buffer, pH 7), at room temperature and without applied potential. After 24 h under an anaerobic atmosphere, only ~10% of the proton reduction activity was lost (Figure S7a,b). However, when kept at applied potential of −0.8 V under otherwise identical conditions, ~90% of proton reduction activity was lost in 22 h (Figure S7a,b). Both conditions were found to have little or no effect on catalytic activity of the enzyme itself (data not shown). At this point it is unclear why an applied, cathodic potential is detrimental to the stability of CaH2ase-based electrodes.

4. CONCLUSION

We have demonstrated dramatic increases in electrocatalytic H_2 production and oxidation currents for electrodes having CaH2ase bound to SWNT networks. In particular, the electrocatalytic activities of the CaH2ase-based electrodes increase with SWNT coverage and m-SWNT content. Improved electrode performance with SWNT networks can be attributed to the effects of m-SWNT on: *i*) CaH2ase electronic coupling with the electrode surface (predominantly at low SWNT coverage) and *ii*) overall electroactive electrode surface available for CaH2ase binding (predominantly at high SWNT coverage).

To our knowledge, this is the first study that demonstrates the effect of SWNT electronic structure on the performance of an enzyme-based electrode. The results demonstrate the potential of m-SWNTs for the construction of highly electroactive surfaces for immobilization of various redox-active biomolecules. Detailed studies of the exact nature of interactions between CaH2ase and SWNT networks as well as further optimization of the system are forthcoming. Such CaH2ase-based electrodes have the potential to enable fabrication of highly electroactive, low-cost, noble-metal-free catalytic electrodes for renewable H_2 conversion devices.

■ ASSOCIATED CONTENT

Supporting Information. (1) Additional SEM figures; (2) background CVs and capacitance measurements; (3) scheme of C-cloth/SWNT/CaH2ase electrode; (4) estimate of H_2 oxidation currents in the absence of mass transfer limitations, Koutecky−Levich plot; (5) electrode stability data; and (6) double layer capacitance data for carbon electrodes. This material is available free of charge via the Internet at http://pubs.acs.org.

■ AUTHOR INFORMATION

Corresponding Author
Paul.King@nrel.gov

■ ACKNOWLEDGMENT

This work was supported through the Laboratory Directed Research and Development program at the National Renewable Energy Laboratory.

■ REFERENCES

(1) Bockris, J. O.; Veziroglu, T. N. *Int. J. Hydrogen Energy* **2007**, *32*, 1605–1610.
(2) Lewis, N. S.; Nocera, D. G. *Proc. Natl. Acad. Sci. U.S.A.* **2006**, *103*, 15729–15735.
(3) Ragnarsdottir, K. V. *Nat. Geosci.* **2008**, *1*, 720–721.
(4) Gordon, R. B.; Bertram, M.; Graedel, T. E. *Proc. Natl. Acad. Sci. U.S.A.* **2006**, *103*, 1209–1214.
(5) Capon, J. F.; Gloaguen, F.; Schollhammer, P.; Talarmin, J. *Coord. Chem. Rev.* **2005**, *249*, 1664–1676.
(6) Justice, A. K.; De Gioia, L.; Nilges, M. J.; Rauchfuss, T. B.; Wilson, S. R.; Zampella, G. *Inorg. Chem.* **2008**, *47*, 7405–7414.
(7) Tard, C.; Pickett, C. J. *Chem. Rev.* **2009**, *109*, 2245–2274.
(8) Vignais, P. M.; Billoud, B. *Chem. Rev.* **2007**, *107*, 4206–4272.
(9) Fontecilla-Camps, J. C.; Volbeda, A.; Cavazza, C.; Nicolet, Y. *Chem. Rev.* **2007**, *107*, 4273–4303.
(10) Vincent, K. A.; Cracknell, J. A.; Clark, J. R.; Ludwig, M.; Lenz, O.; Friedrich, B.; Armstrong, F. A. *Chem. Commun.* **2006**, 5033–5035.
(11) Hambourger, M.; Gervaldo, M.; Svedruzic, D.; King, P. W.; Gust, D.; Ghirardi, M.; Moore, A. L.; Moore, T. A. *J. Am. Chem. Soc.* **2008**, *130*, 2015–2022.
(12) Armstrong, F. A.; Belsey, N. A.; Cracknell, J. A.; Goldet, G.; Parkin, A.; Reisner, E.; Vincent, K. A.; Wait, A. F. *Chem. Soc. Rev.* **2009**, *38*, 36–51.
(13) Alonso-Lomillo, M. A.; Rudiger, O.; Maroto-Valiente, A.; Velez, M.; Rodriguez-Ramos, I.; Munoz, F. J.; Fernandez, V. M.; De Lacey, A. L. *Nano Lett.* **2007**, *7*, 1603–1608.
(14) Willner, B.; Katz, E.; Willner, I. *Curr. Opin. Biotechnol.* **2006**, *17*, 589–596.
(15) Chen, D.; Wang, G.; Li, J. H. *J. Phys. Chem. C* **2007**, *111*, 2351–2367.
(16) North, S. H.; Lock, E. H.; Taitt, C. R.; Walton, S. G. *Anal. Bioanal. Chem.* **2010**, *397*, 925–933.
(17) Lojou, E.; Luo, X.; Brugna, M.; Candoni, N.; Dementin, S.; Giudici-Orticoni, M. T. *J. Biol. Inorg. Chem.* **2008**, *13*, 1157–1167.
(18) Luo, X. J.; Brugna, M.; Tron-Infossi, P.; Giudici-Orticoni, M. T.; Lojou, E. *J. Biol. Inorg. Chem.* **2009**, *14*, 1275–1288.
(19) Hoeben, F. J. M.; Heller, I.; Albracht, S. P. J.; Dekker, C.; Lemay, S. G.; Heering, H. A. *Langmuir* **2008**, *24*, 5925–5931.
(20) Liu, A. R.; Wakayama, T.; Nakamura, C.; Miyake, J.; Zorin, N. A.; Qian, D. J. *Electrochim. Acta* **2007**, *52*, 3222–3228.
(21) Le Goff, A.; Artero, V.; Jousselme, B.; Tran, P. D.; Guillet, N.; Metaye, R.; Fihri, A.; Palacin, S.; Fontecave, M. *Science* **2009**, *326*, 1384–1387.
(22) Gooding, J. J.; *Electrochim. Acta* **2005**, 3049−3060.
(23) Banks, C. E.; Davies, T. J.; Wildgoose, G. G.; Compton, R. G. *Chem. Commun.* **2005**, 829–841.
(24) McDonald, T. J.; Svedruzic, D.; Kim, Y. H.; Blackburn, J. L.; Zhang, S. B.; King, P. W.; Heben, M. J. *Nano Lett.* **2007**, *7*, 3528–3534.
(25) Blackburn, J. L.; Svedruzic, D.; McDonald, T. J.; Kim, Y. H.; King, P. W.; Heben, M. J. *Dalton Trans.* **2008**, 5454–5461.
(26) Arnold, M. S.; Green, A. A.; Hulvat, J. F.; Stupp, S. I.; Hersam, M. C. *Nat. Nanotechnol.* **2006**, *1*, 60–65.
(27) Harnisch, F.; Sievers, G.; Schroder, U. *Appl. Catal., B* **2009**, *89*, 455–458.

(28) Cracknell, J. A.; Vincent, K. A.; Armstrong, F. A. *Chem. Rev.* **2008**, *108*, 2439–2461.
(29) Beard, M. C.; Blackburn, J. L.; Heben, M. J. *Nano Lett.* **2008**, *8*, 4238–4242.
(30) Blackburn, J. L.; Barnes, T. M.; Beard, M. C.; Kim, Y. H.; Tenent, R. C.; McDonald, T. J.; To, B.; Coutts, T. J.; Heben, M. J. *ACS Nano* **2008**, *2*, 1266–1274.
(31) Tenent, R. C.; Barnes, T. M.; Bergeson, J. D.; Ferguson, A. J.; To, B.; Gedvilas, L. M.; Heben, M. J.; Blackburn, J. L. *Adv. Mater.* **2009**, *21*, 3210–+.
(32) Selig, M. J.; Viamajala, S.; Decker, S. R.; Tucker, M. P.; Himmel, M. E.; Vinzant, T. B. *Biotechnol. Prog.* **2007**, *23*, 1333–1339.
(33) King, P. W.; Posewitz, M. C.; Ghirardi, M. L.; Seibert, M. *J. Bacteriol.* **2006**, *188*, 2163–2172.
(34) Barton, S. C.; Sun, Y. H.; Chandra, B.; White, S.; Hone, J. *Electrochem. Solid State Lett.* **2007**, *10*, B96–B100.
(35) Barbieri, O.; Hahn, M.; Herzog, A.; Kotz, R. *Carbon* **2005**, *43*, 1303–1310.
(36) Gao, G. H.; Cagin, T.; Goddard, W. A. *Nanotechnology* **1998**, *9*, 184–191.
(37) Peigney, A.; Laurent, C.; Flahaut, E.; Bacsa, R. R.; Rousset, A. *Carbon* **2001**, *39*, 507–514.
(38) Kinoshita, K. *Carbon:Electrochemical and Physicochemical Properties*: John Wiley and Sons: New York, 1988.
(39) Vincent, K. A.; Parkin, A.; Armstrong, F. A. *Chem. Rev.* **2007**, *107*, 4366–4413.
(40) Peters, J. W.; Lanzilotta, W. N.; Lemon, B. J.; Seefeldt, L. C. *Science* **1998**, *282*, 1853–1858.
(41) Leger, C.; Bertrand, P. *Chem. Rev.* **2008**, *108*, 2379–2438.
(42) von Abendroth, G.; Stripp, S.; Silakov, A.; Croux, C.; Soucaille, P.; Girbal, L.; Happe, T. *Int. J. Hydrog. Energy* **2008**, *33*, 6076–6081.